Ultrasonics Sonochemistry 95 (2023) 106411

Contents lists available at ScienceDirect

Ultrasonics Sonochemistry

journal homepage: www.elsevier.com/locate/ultson

Ultrasonic enhancement of microdroplet-based interfacial reaction for improving the synthesis of Ag_2S QDs

Zongbo Zhang [a,*], Changbin Xu [a], Shiliang Song [a], Yan Ding [a], Nan Meng [a], Xuesheng Liu [a], Yuan Zhang [c], Liang Gong [c], Wenting Wu [b,*]

[a] College of Mechanical and Electrical Engineering, China University of Petroleum (East China), Qingdao 266580, PR China
[b] State Key Laboratory of Heavy Oil Processing, China University of Petroleum (East China), Qingdao 266580, PR China
[c] College of New Energy, China University of Petroleum (East China), Qingdao 266580, PR China

ARTICLE INFO

Keywords:
Ultrasound
Microdroplet
Interfacial reaction
Mass transfer
Ag_2S QDs

ABSTRACT

Ag_2S quantum dots (QDs) have aroused extensive concerns in intravital imaging field due to their merits of narrow bandgap, low biological toxicity and decent fluorescence emission properties in the second near-infrared (NIR-II) window. However, low quantum yield (QY) and poor uniformity of Ag_2S QDs are still main obstacles for its application. In this work, a novel strategy of utilizing ultrasonic field is presented, which can enhance the microdroplet-based interfacial synthesis of Ag_2S QDs. The ultrasound increases the presence of ions at the reaction sites by enhancing the ion mobility in the microchennels. Therefore, the QY is enhanced from 2.33 % (optimal QY without ultrasound) to 8.46 %, which is the highest value of Ag_2S ever reported without ion-doping. Also, the decrease of the corresponding full width at half maximum (FWHM) from 312 nm to 144 nm indicates the obvious uniformity improvement of the obtained QDs. Further mechanism exploration illustrates that ultrasonic cavitation significantly increases the interfacial reaction sites by splitting the droplets. Meanwhile, the acoustic flow field strengthens the ion renewal at the droplet interface. Consequently, the mass transfer coefficient increases by more than 500 %, which is favorable to improve both the QY and quality of Ag_2S QDs. This work serves both fundamental research and practical production for the synthesis of Ag_2S QDs.

1. Introduction

Cell imaging and vivo fluorescent probes based on QDs are considered as the next-generation imaging techniques to uphold the booming of life sciences [1–3]. Considering the high demands on resolution, penetration depth and biocompatibility, Ag_2S QDs have been intensively studied due to their merits such as narrow bandgap, low biological toxicity and decent fluorescence emission properties in NIR-II (1000–1700 nm) window where body autofluorescence and photon scattering are especially low, resulting in significant improvement in imaging resolution (micrometer-scale) and light penetration depth (up to several millimeters) [4–8]. Although many routines for the preparation of Ag_2S QDs have emerged, most of them suffer from low QY and deficient crystal structure, which are mainly caused by superfluous cation vacancies and crystal defects originated from the excessive mobility of Ag^+ in the crystal lattice [9,10].

In order to improve the above situation, numerous studies from traditional batch-based reaction to continuous microreaction have been reported in recent years as shown in Fig. 1. For example, Wang et al. synthesized Ag_2S QDs by one-pot method in ordinary chemical glassware. The QY of the prepared QDs was 1.8 % with the average diameter of 2.1 ± 0.3, which was evidently low for biological application [11]. He et al. prepared the Ag_2S QDs with QY of 4.5 % and nanocrystal size of 2.8 ± 0.4 nm in a three-necked flask. Then, they further doped Pb^{2+} ions into the as-obtained QDs to improve the QY. Actually, doping the host crystals by transition metal ions (Zn^{2+}, Cd^{2+}, Hg^{2+}, Mn^{2+}) to raise the QY was widely studied in previous researches, however the introduction of heavy metals usually challenges the biocompatibility of the host Ag_2S QDs [9,10,12,13]. Although the above macroscopic batch-based reactions are simple, it is difficult to precisely control the synthesis process resulting in poor consistency and low QY [1].

Actually, continuous microreaction is promising in accurate regulation of chemical reaction benefitting from its minute reaction size. Some attempts also have been made to utilize microreactor in the synthesis of Ag_2S QDs [14]. Bhanu Prakash et al. synthesized QDs in milliliter-scale microchannels [15]. Whereas, the slower mass transfer in the laminar-

* Corresponding authors.
E-mail addresses: zzb001_0@163.com (Z. Zhang), wuwt@upc.edu.cn (W. Wu).

https://doi.org/10.1016/j.ultsonch.2023.106411
Received 9 February 2023; Received in revised form 9 April 2023; Accepted 17 April 2023
Available online 19 April 2023

flow dominated microchannel resulted in less new nucleation of crystals, and larger the average size of QDs (about 15 nm) which severely exceeded the natural filtration threshold in living organisms (5 nm) [16]. To improve the mass transfer efficiency in the microreaction system, Shu et al. presented a microdroplet reactor for synthesizing Ag_2S QDs. In this process, the precursors were wrapped in droplets which were dispersed in the continuous phase within microchannels. And the synthesis reaction took place only in microliter-sized droplets. The size of the obtain QDs was well controlled in the range of 2.3–3.5 nm with QY of 3 % [17].

Although the limited volume of microdroplets could ameliorate the nucleation and restrict the excessive crystal growth in this method, the limitation of the reactants in such small droplets also affects the growth and development of QDs and results in defects such as multi-peak emission. Zeng et al. further explored the microdroplet reaction system and moved the reaction to the surface of the droplet. In this process, one precursor was in the continuous phase (outside the droplet) and the other precursor was in the dispersed phase (inside the droplet), so the synthesis reaction took place at the interface of the droplet. At the same time, the flow of the droplet in the microchannel promoted the renewal of ions at the interface, which could ameliorate the defects derived from the excessive mobility of Ag^+ in the crystal lattice. Thus, the fluorescence spectra of obtained QDs was a clear single-peak emission, which indicated significant less defects in the crystal. Moreover, the average diameter of the obtained QDs was well controlled in the range of 1.70–1.85 nm [18]. These excellent QDs properties showed the unique advantage in precise regulation of the synthesis process in this method. However, the limited surface area and passive convection inside the droplets caused some disadvantages such as slow reaction rate and low QY (2.91 %) which greatly affected its large-scale production and industrial applications. Overall, effective regulation of the reaction process is vital for achieving high quality and yield during preparation of QDs, which is especially difficult for such small synthesis units in microdroplet reactor.

In this work, an interfacial reaction based ultrasonic microdroplet reactor for effectively synthesizing of Ag_2S QDs in room temperature is presented. The ultrasonic energy is transferred by the direct coupling of microdroplet reactor and ultrasonic transducer. The evolution of the droplets and the flow field around them is studied to explore the mechanism of ultrasonic enhancement in this microdroplet reaction via high speed photography and particle image velocimetry (PIV) experiments. The whole interfacial reaction process is benefited from the increasing specific surface area of droplets and the violent disturbance of the flow field in microchannels. In addition, this paper confirms the significant enhancement and effective regulation of ultrasound in the synthesis of QDs, which is beneficial to both fundamental research and practical large-scale production of Ag_2S QDs.

2. Materials and experiments

2.1. Fabrication and characterization of ultrasonic microdroplet reactor

The microdroplet reactor is fabricated using polymethyl methacrylate (PMMA) substrates with thickness of 2 mm. In the reactor, the width and depth of the main channel are both 800 μm, while the width and depth of the flow-focusing throat are 200 μm and 800 μm respectively. The structure is used to generate continuous and controllable microdroplet, and the interfacial reaction occurs on the surface of the microdroplet, as shown in Fig. 2a. Nucleation and growth of Ag_2S QDs as shown in Fig. 2b. In the process of experiment, the color of the droplets gradually changed from colorless to dark brown with the reaction proceeded, which is related to the growth of QDs, as shown in Fig. 2. 2-

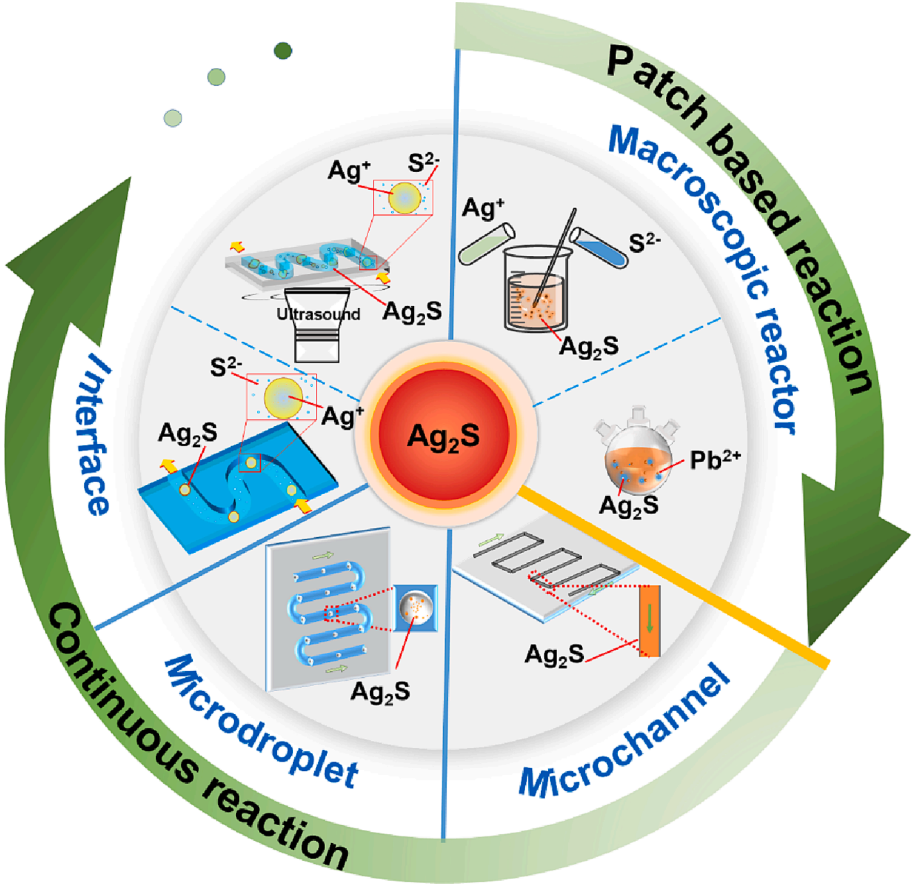

Fig. 1. Schematic illustration of the development for synthesis of Ag_2S QDs.

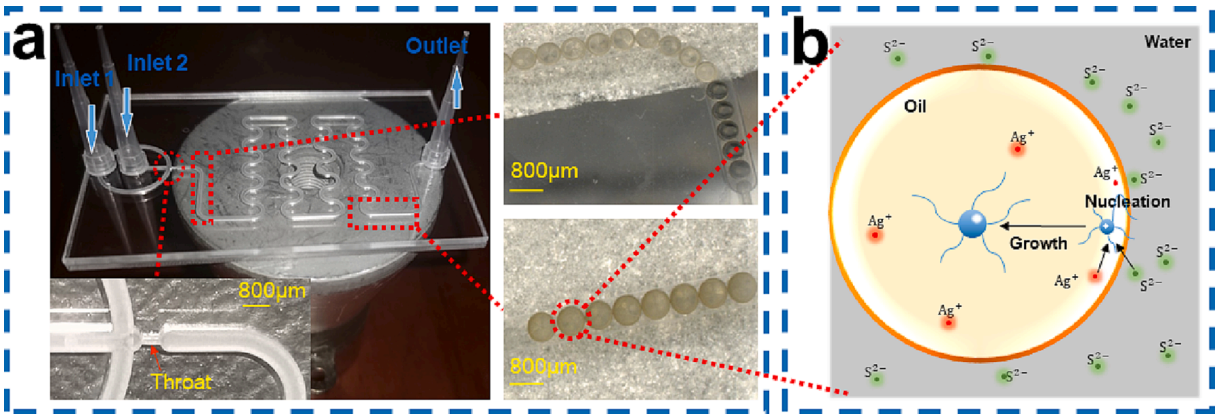

Fig. 2. (a) Photographs of microstructures in different locations of the reactor. (b) Schematic diagram of interfacial reaction in the microdroplet reactor.

Propanol (AR , ≥ 99.7 % , China) is used as solvent to bond the substrates. As shown in Fig. 3, the ultrasonic transducer (220-DG1, 60 W, Fukang, China) directly bonded with the bottom surface of the microdroplet reactor. The whole device is controlled by shock absorber.

In the experimental process, the water and oil phases are the continuous and dispersed phases, respectively. In order to form stable O/W droplets, a hydrophilic film is formed by hydrophilic modification of the inner wall surface of the microchannel, and the detailed procedure and droplet contact angle experiments are described in part 1 of supplementary. Two injection pumps (SPC, Easypump, China) and the microdroplet reactor are connected by PTFE tubes (ID 0.8 mm, OD 1 mm) and the flow rate of both phases are governed by a master control platform (SN-003, Shenchen pump industry, China). Two ultrasonic transducers with the same power of 60 W and different frequency of 28 kHz and 40 kHz are employed in the experiment to explore the specific effects of ultrasonic frequencies on the properties of Ag_2S QDs. A self-made cooling device is used to control the temperature of the transducer.

The microdroplets and flow fields are observed and recorded by high-speed camera (FASTACAM NOVAS12, Photron , Japan) connected with microscope(Nikon MA200, Japan) and PIV system (Flowmaster MITAS, LaVision. Ltd, USA). In the high-speed photography, the frame rate is 16,000 fps (exposure time is 1/60,000 s) with the resolution of 1024 × 1024 pixels and the magnification of 100. PIV experiment is carried out by dispersing fluorescent polystyrene microspheres (Fluoro-Max , Thermo scientific, USA) with diameter of 0.76 μm.

2.2. Materials and synthesis of Ag_2S QDs

Sodium sulfide nonahydrate ($Na_2S \bullet 9H_2O$, 99.99 %), Octadecene (ODE, > 90 %), Oleic acid (OAc, AR), Oleylamine (OAm, AR, 80 % −90 %), Tween 20, Ethanol (C_2H_5OH, ACS, ≥ 99.5 %), Tetrachloroethylene (C_2Cl_4, ≥ 99.5 %) are purchased from Aladdin Chemistry Co. Ltd (Shanghai, China). Silver acetate (AgAc, AR, 99.5 %) , Indocyanine green (ICG, AR), Dimethylsulfoxide (DMSO) are purchased from Shanghai Macklin Biochemical Co. Ltd. Ultrapure water from Ultrapure water system (Minbase-2041 T). The above reagents can be used without further purification.

AgAc (8.4 mg) is added to a mixture solution consisting of ODE (4.25 mL), OAc (0.25 mL), OAm (0.5 mL) to prepare the silver precursor. $Na_2S \bullet 9H_2O$ (3.0 mg, 4.0 mg, 5.0 mg, 6.0 mg, 7.0 mg) is dissolved in 11.16 mL of ultrapure water containing a certain volume fraction of Tween 20 to prepare the sulfur precursor, respectively. Subsequently, the two precursor solutions are stirred at room temperature until they get completely transparent. During the experiment, the sulfur precursor solution is the continuous phase with the volume flow rate set to 75 μL / min (Qc), while the silver precursor solution is the dispersed phase with the volume flow rate set to 37.5 μL / min (Qd).

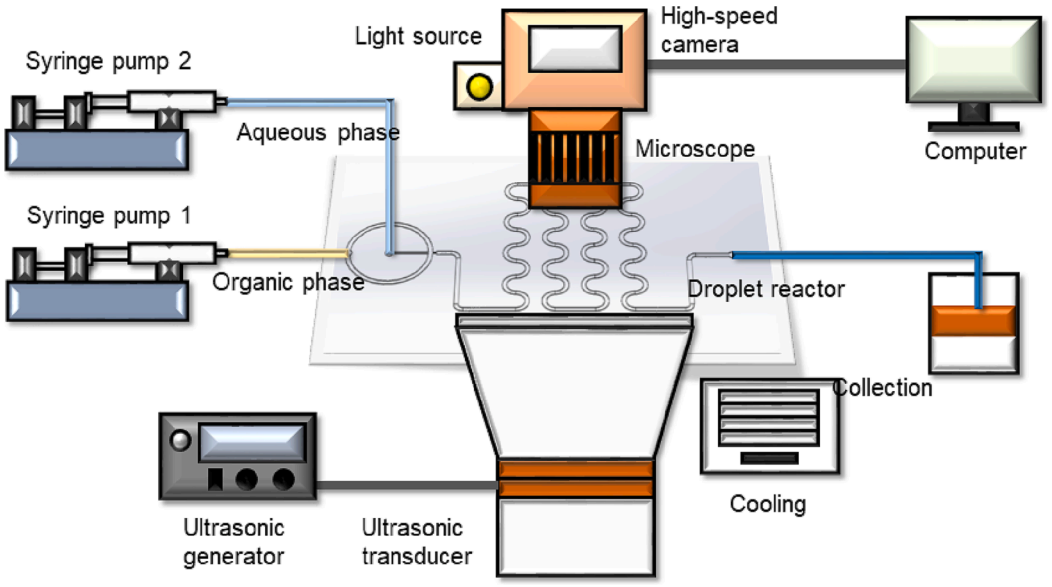

Fig. 3. Schematic diagram of ultrasonic enhanced microdroplet reaction system.

2.3. Collection and characterization of Ag_2S QDs

The obtained unstratified product is centrifuged at 8000 rpm for 5 min in a benchtop high-speed centrifuge (TG 16 - WS), and then the upper oil phase containing Ag_2S QDs is transferred to a new centrifuge tube. A sufficient amount of anhydrous ethanol is added to the centrifuge tube and sonicated for 3 min during the process. Repeat the above operation 2 ~ 3 times to obtain pure Ag_2S QDs.

The above precipitates are dispersed into C_2Cl_4 solution. The UV absorption spectra and fluorescence spectra of QDs are recorded on UV spectrophotometer (UV-2700, Shimadzu, Japan) and fluorescence spectrophotometer (FLS 980, Edinburgh Instruments, UK), respectively. Transmission electron microscope images (TEM) and high-resolution TEM images (HR-TEM) are obtained on transmission electron microscope (JEM-2100, JOEL, Japan). XPS images are obtained from tests in X-ray photoelectron spectrometer (ESCALAB 250 Xi, Thermo Fisher

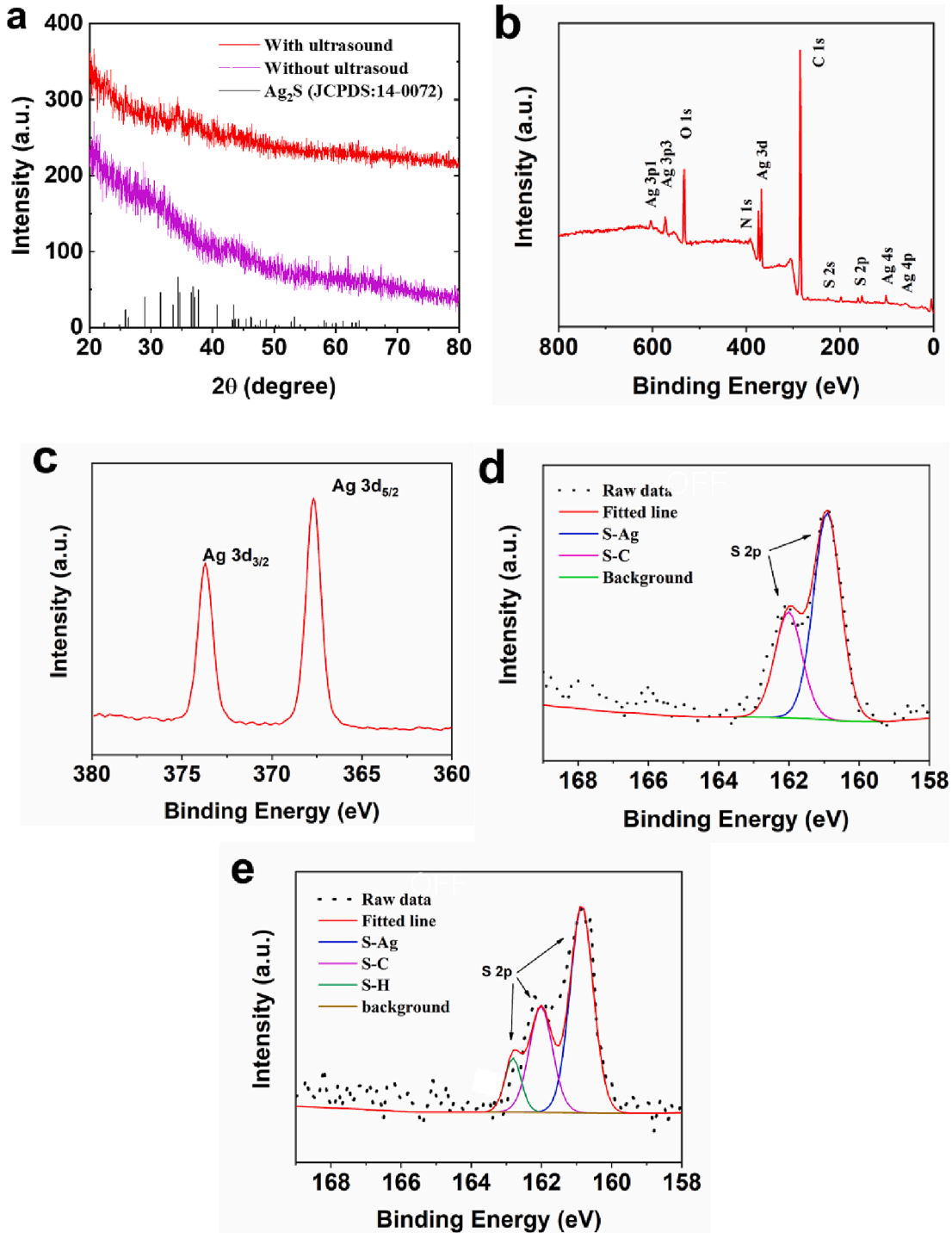

Fig. 4. Characterization of Ag_2S QDs at molar ratio of 12: 5. (a) XRD patterns (with and without ultrasound). (b) The full spectrum of XPS and the corresponding high resolution spectrum of Ag_2S QDs under ultrasonic radiation at room temperature. (c) Ag 3d. (d) S 2p. (Qc = 75 μL / min, Qd = 37.5 μL / min). (e) The XPS image of S^{2-} at 12: 7.

Scientific, UK). XRD images are obtained from X-ray diffractometer (D8 Advance, Bruker, Germany). The concentration of sulfide ions in the solution is recorded by Inductively coupled plasma spectrometer (Agilent5110, Agilent Technologies, USA).

3. Results and discussion

3.1. Effects of ultrasound on the properties of Ag_2S QDs

In order to illustrate that ultrasound only affects the performance

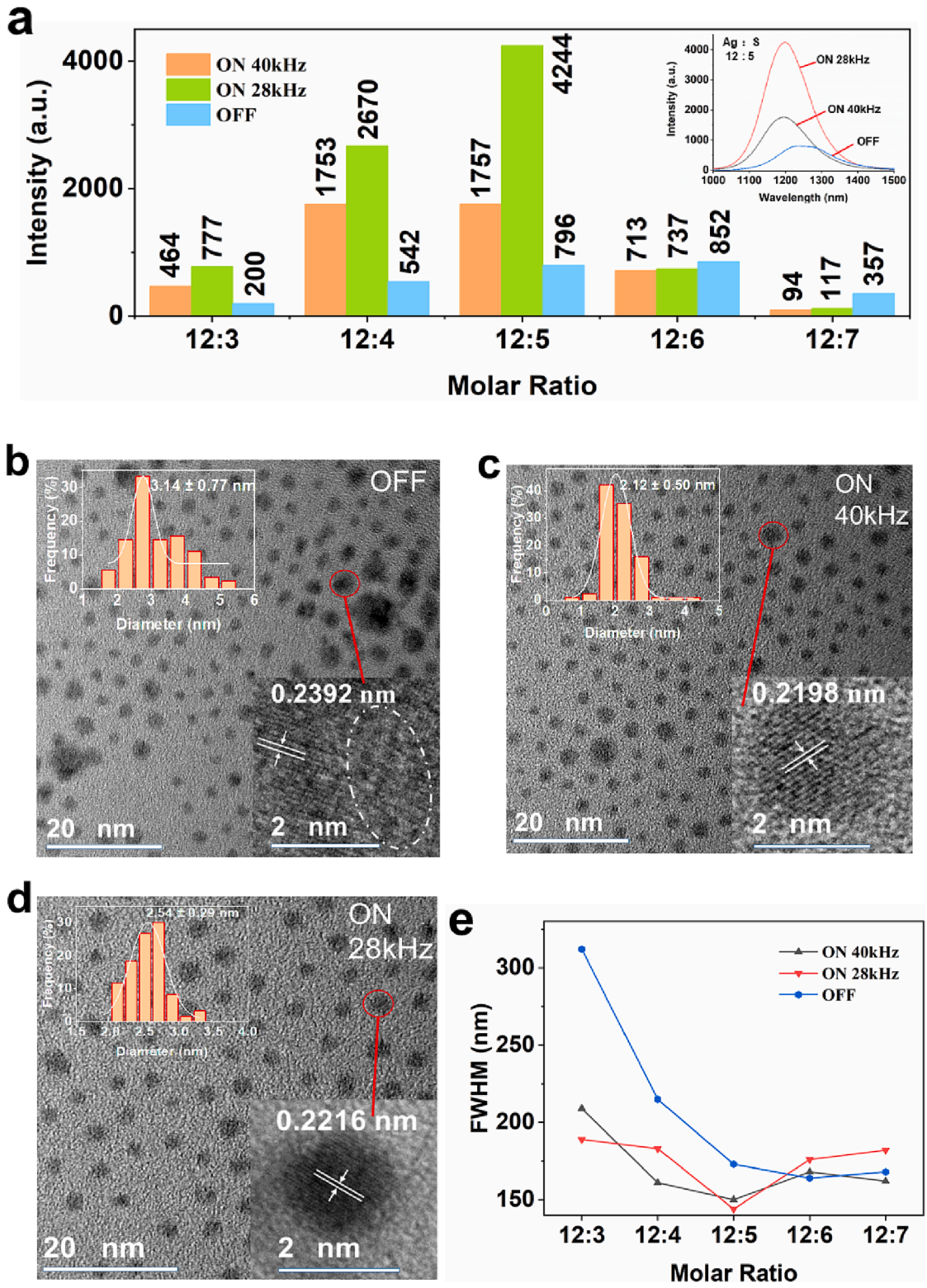

Fig. 5. (a) Fluorescence intensity of QDs with different molar ratios under ultrasound (The inset figure shows the fluorescence emission spectrum of Ag_2S QDs under 12: 5). (b), (c), (d) TEM images and histograms of particle size distribution of Ag_2S QDs at different frequencies of ultrasound at 12: 5 M ratio and the corresponding HR - TEM images, respectively. (e) FWHM of QDs fluorescence peaks under different molar ratios.

characteristics of QDs and without formation of other substances, XRD and XPS tests are carried out. The corresponding results are shown below. Fig. 4a shows the crystal structure of the obtained Ag_2S QDs with and without ultrasound. With the radiation of ultrasonic, the nanocrystals gradually appeared obvious diffraction peaks, which is attributed to monoclinic Ag_2S (JCPDS:14-0072). The relatively strong diffraction peaks at 2θ around 34.39°, 37.72°and 43.41°are corresponded to the (−1 2 1), (−1 0 3) and (2 0 0) crystal planes in Ag_2S QDs, respectively. Likewise, the XRD pattern clearly shows that no diffraction peaks are detected in other positions, which proves that prepared nanocrystals have good purity. XPS testing can be used to determine the elemental composition and chemical status of QDs. It can be seen from the full spectrum of Fig. 4b that the prepared Ag_2S QDs is composed of Ag, S, C, N and O elements. In the high-resolution spectrum of Ag 3d (Fig. 4c), 367.6 and 373.9 eV correspond to Ag 3d5/2 and Ag 3d3/2 in QDs, respectively. The S 2p peaks at 161.2 and 162.4 eV correspond to S-Ag and S-C, respectively (Fig. 4d) [9,11]. The above results confirmed that the Ag_2S QDs is successfully synthesized without introduction of other chemical product via the interfacial reaction under the radiation of ultrasonic in microdroplet reactor.

Fig. 5a shows the influence of the ultrasound and reactant ratio on the fluorescence intensity of Ag_2S QDs. The fluorescence intensity increases first and then decreases with the rise of the molar ratio. The detailed results of the QDs obtained at low S^{2-} concentrations (molar ratios of 12:3 and 12:4) are analyzed as follows. Without ultrasonic radiation, the fluorescence emission spectra are unsymmetrical multiple-emission curves with quite low peaks (Fig. S3a and S3b), which is obvious different from typical QDs emission of binary structure. In this case, the high Ag^+ mobility in the nanocrystals [9,10,19] and the lack of S^{2-} result in numerous structural defects in QDs and multiple emission [20]. With ultrasonic radiation, the fluorescence emission peak type of QDs tends to be single symmetrical emission with narrower FWHM (Fig. 5e) [21–23]. The fact is also supported by the TEM test as shown in Fig. S4a and S4b. Compared with the QDs without ultrasonic radiation, the shape and the distribution of the QDs obtained with ultrasound are more uniform. Overall, the introduction of ultrasound accelerates the renewal rate of the reactants, thus alleviating the shortage of S^{2-} on the droplet interface when the concentration of S^{2-} is low [24].

When the concentrations of S^{2-} are relatively high (molar ratios of 12: 6 and 12: 7), the fluorescence intensity decreases and the QDs size (from 3.32 nm to 4.59 nm) increases with the rise of the molar ratio (Fig. 5a and Fig. S3c and S3d). This result is mainly due to excessive S^{2-} which disturbs the self-assembled process of the QDs and results in the degradation of the crystal structure and optical quality of QDs [25,26]. This result is also supported by visible larger and less uniform QDs in Fig. S4d compared with that in Fig. S4c. With ultrasonic radiation, the fluorescence intensity of QDs further decreases and multi-peak emission appears (Fig. S3c and S3d). In this process, the ultrasound accelerates the renewal of the interface reaction, which results in local excessive of S^{2-} and explosive growth of the QDs. Therefore, it is difficult for QDs to maintain their original structure, thereby triggering self-quenching effect caused by aggregation [27]. Comparing the XPS images of Ag: S = 12: 7 (Fig. 4e) and that of Ag: S = 12: 5 (Fig. 4d), the appearance of the S-H suggests that excess S^{2-} attaches on the surface of QDs in form of hydrosulfide [28].

Above all, the ultrasound increases the presence chance of S^{2-} at the reaction site by enhancing the mobility of S^{2-} in the reaction, which can compensate the ion shortage when the concentration of S^{2-} is low but deteriorate the over-growth of the crystal when the concentration of S^{2-} is excessive. Therefore, the optimization of ion concentration is vital for the quality of QDs in this method. The optimal fluorescence intensities achieved at Ag: S = 12: 5 with ultrasound and at Ag: S = 12: 6 without ultrasound, respectively. Remarkably, the fluorescence intensity increases by about 400 % with ultrasound frequency of 28 kHz (at molar ratio of 12: 5) compared with that without ultrasound (at molar ratio of 12: 6). The corresponding QY reaches 8.46 % which is the highest values ever reported for NIR-II Ag_2S QDs (Table 1) [4,9–11,17,18,29].

Table 2 shows the detailed data of the obtained QDs at molar ratio of 12: 5. The atomic ratio of Ag and S in the nanoparticles is much closer to the stoichiometric ratio of Ag_2S under the radiation of ultrasound, which implies more optimal element composition in the QDs. Especially, the atomic ratio of Ag and S reaches 2.03 at frequency of 28 kHz, which is almost equal to the theoretical value (2.0). This is because ultrasound can improve the ion concentration distribution both inside and outside the droplets. On the one hand, ultrasound can promote the movement of Ag^+ inside the droplet from high concentration to the interface where Ag^+ is consumed, thus improving the homogeneity of Ag^+. On the other hand, ultrasound can speed up the position change of microdroplets in the channel, thus compensating the supplementary of S^{2-} on the droplet surface.

As shown in the TEM images in Fig. 5, the size of the QDs prepared in ultrasonic field is more uniform, and the shape is closer to a circle than those obtained without the ultrasonic radiation. Specifically, the lattice fringes in HR-TEM image of Fig. 5b are fuzzy and fragmentary or even disappeared in some location (as shown inside the elliptical dotted line), which illustrates poor crystallinity and visible defects in the QDs obtained without the ultrasound. With ultrasonic radiation, the lattice fringes with favorable integrity can be easily observed in HR-TEM image of Fig. 5c and Fig. 5d, which indicated the improvement of the crystallization process by ultrasound.

In brief, the excellent performance of the QDs obtained with ultrasonic radiation is mainly attributed to the optimization of quantum dot composition [20] and lattice integrity [30,31]. In this process, the ultrasound changes the droplet morphology and the flow field to achieve the above improvement. These changes can not only provide more sites for the synthesis of nanocrystals by increasing the specific surface area of droplet, but also improve the uniformity of crystal nucleus formation by vigorous stirring effect [14].

3.2. Ultrasonic influence mechanism

PIV and high-speed camera experiments are further carried out to reveal the droplet behavior and its influence on the above interfacial reaction. As shown in video S1, both the steady-state cavitation bubbles and the transient cavitation bubbles form in the continuous phase (water phase) rather than in the dispersed phase (oil phase), which is mainly attributed to low viscosity and high gas solubility in water [32–34]. As shown in Fig. 6a and video S1a, the radius of the steady-state cavitation bubble is usually larger than the resonance radius(125 μm)so these bubbles mainly oscillate in size [35]. As these bubbles approach to a droplet, the oscillating bubbles not only excite the oscillation of the droplet wall but also squeeze the droplet in the channel resulting in obvious deformation, both of which obviously change the flow field in the vicinity of the droplet interface. Fig. 6b and video S1b show the effect of the transient-cavitation-bubble collapse on a droplet. Under the ultrasonic radiation, the small bubbles (smaller than resonance size) grow to the resonance size then collapse in a very short time. The collapse of the bubble generates powerful shock waves and high-speed micro-jets in a very local area, resulting in violent nonlinear flow

Table 1
Comparison of various methods to synthesize Ag_2S QDs.

Method	Temperature (℃)	Emission (nm)	Size (nm)	QY (%)	Ref.
Interface	Room temp	1195–1262	1.8–6.2	8.46	This work
Solution	37	650–850	2.1–2.4	1.8	[11]
Solution	165	975–1242	2.7–2.8	4.5	[10]
Solution	Room temp	1050–1294	1.6–6.8	1.8	[4]
Solution	145	510–1221	1.5–6.3	2.1	[29]
Solution	145	955–1200	3.5–5.8	4.14	[9]
Droplet	81–117	552–874	2.1–2.9	3	[17]
Interface	Room temp	662–680	1.7–1.8	2.91	[18]

Table 2
Product characteristics for different conditions at molar ratio of 12: 5.

Reaction condition	Size (nm)	Size dispersity (%)	Atomic ratio of Ag to S	QY (%)
ON 40 kHz	2.12	77.27	2.28	3.92
ON 28 kHz	2.54	44.99	2.03	8.46
OFF	3.14	47.78	1.36	2.54

disturbance. The collapsed bubble generates numerous microbubbles (microbubble cluster), which gather, grow and collapse again. When the collapsing bubble is not close enough to a droplet, the collapse-induced disturbance directly deforms the droplet leading to the change of the flow field both in and out the droplet. As the droplet approaches closer to the collapse region, it is quickly dragged into the collapse region and teared into much smaller microdroplets by the shock waves and micro-jets, which dramatically increase the interface of the droplet thereby multiply the interface reaction sites.

In order to quantitatively evaluate the breaking effect of transient cavitation, we conduct the particle size analysis experiments on the droplets under ultrasonic radiation with different frequencies, as shown in Fig. 7. The average size of the obtained microdroplets without ultrasound is 200 μm (depending on the flow-focusing structure). After ultrasound treatment, the average size of the microdroplets are 500 nm (40 kHz) and 250 nm (28 kHz), respectively, which are three orders smaller than that without ultrasound. This result is significantly favorable for increasing the surface area of the droplets, which provides more ion reaction sites for the interface synthesis.

Fig. 8 displays the velocity field in the microchannel obtained from PIV test. The velocity of the fluid in the microchannel without ultrasound illustrates a pretty uniform flow rate (Fig. 8a), which indicates typical laminar-dominated flow [36]. In this case, the reactants are mainly mixed by molecular diffusion, thus leading to low diffusion rate.

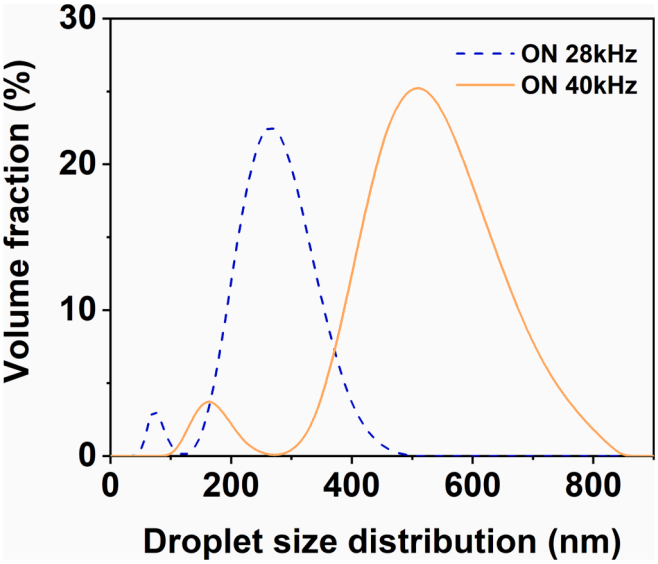

Fig. 7. Droplet size distribution under the radiation of ultrasound at room temperature (Qc = 75 μL / min, Qd = 37.5 μL / min).

Fig. 8b and 8c show the velocity fields in the microchannel with ultrasound at the frequency of 40 kHz and 28 kHz, respectively. The radiation of ultrasound can cause disturbance in the microchannel, which generate obvious vortices. This disturbance mainly comes from the direct sound flow and the behavior of cavitation bubbles under the radiation of ultrasound (video S1). Consequently, the vortices with the ultrasound frequency of 28 kHz are more obvious than that of 40 kHz (shown in Fig. 8c and 8b), as the amplitude of the former is larger than

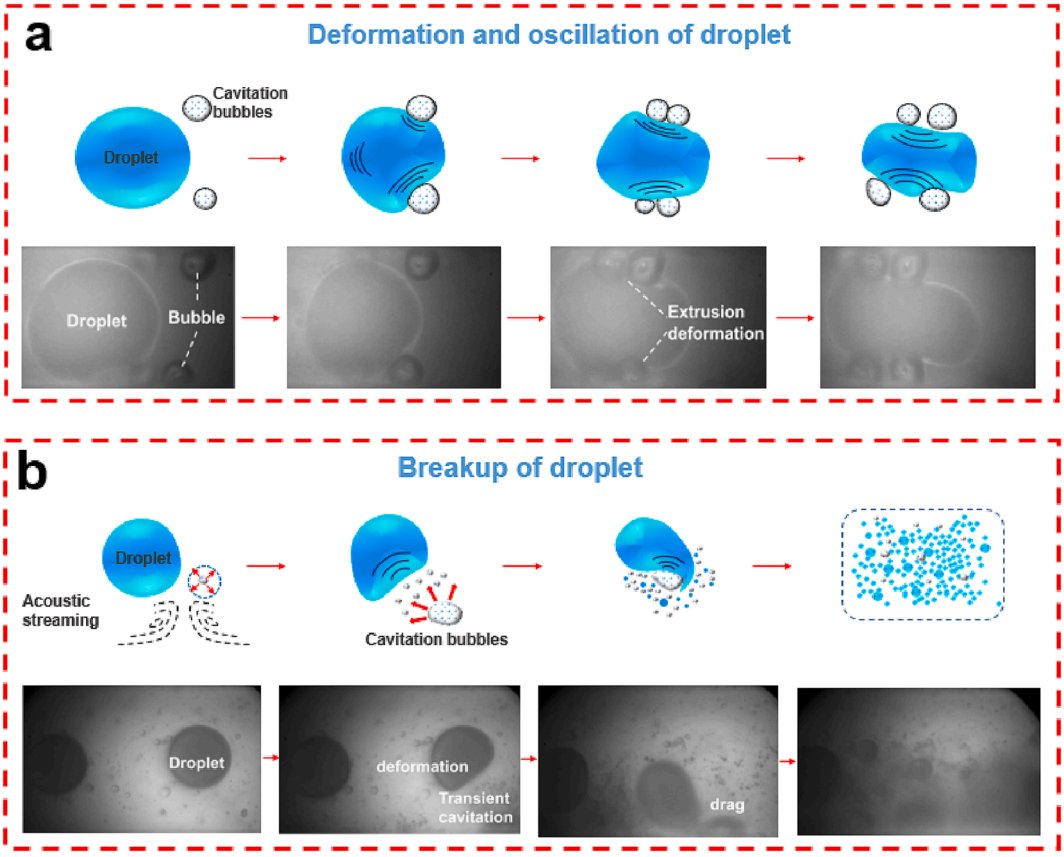

Fig. 6. (a) Effect of steady-state cavitation on droplet. (b) Effect of transient cavitation on droplet.

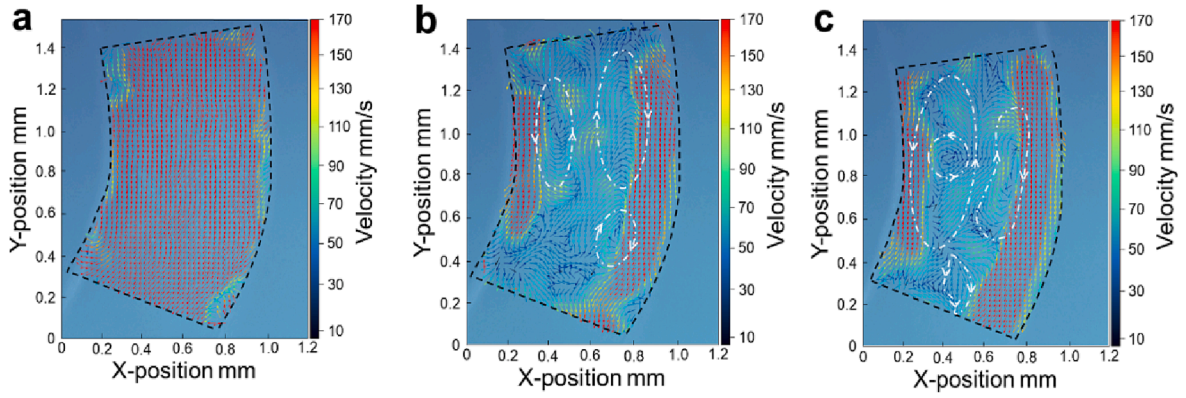

Fig. 8. PIV results of flow field in microchannel (a) without ultrasonic radiation, (b) under the radiation of 40 kHz ultrasound and (c) under the radiation of 28 kHz ultrasound (Black dashed refers to microchannel).

the latter. These ultrasound-induced vortices significantly enhance the mass transfer process of the medium in the microchannel. In addition, our previous work had also revealed that the ultrasonic field could also remarkably promote the mass transfer inside the droplet [37]. Therefore, the mass transfer enhancement of both inside and outside the droplet accelerates the ion renewal rate on the reaction interface.

To further characterize the mass transfer enhancement in the microchannel, we calculate the mass transfer coefficient with the following formula [38,39]:

$$\mathrm{Kla} = \frac{1}{\tau}\ln\frac{Ci - Ca}{Co - Ca}$$

where τ represents the average residence time of the liquid in microreactor, *Ci*, *Co* and *Ca* are concentrations of sulfide ions at inlet, outlet, and equilibrium, respectively.

As shown in Fig. S5, compared with that without ultrasound, the mass transfer coefficient is dramatically increased by 526.86 % and 339.93 % with the ultrasonic frequency of 28 kHz and 40 kHz, respectively. This result further proved the significant enhancement of the ultrasonic radiation for the mass transfer process of the above droplet reaction system. Therefore, the uniformity and yield of silver sulfur QDs based on the interface reaction were dramatically improved by the coupling of ultrasound and microdroplets.

4. Conclusion

In this paper, we propose an interfacial-reaction based synthesis method to improve the QY and properties of Ag_2S QDs by coupling the ultrasound with microdroplet in a micro reactor. The obtained QDs show excellent performance in QY (8.46 %), size uniformity (FWHM of 144 nm) and crystal structures, which provides strong support in the application of bioimaging. Subsequently, the enhancement of ultrasound on microdroplet interfacial reaction is explored. The splitting of microdroplets caused by transient ultrasonic cavitation significantly increases the sites for ion contact in the interfacial reaction (droplet diameter is reduced from 200 μm to 250 nm), which alleviates the limiting effect of the single droplet interface on the nucleation and growth of QDs. Furthermore, the acoustic flow field inside the microchannel strengthens the ion renewal at the droplet interface. The above effects of ultrasound consequently intensify the mass transfer coefficient by 526.86 % compared with that without ultrasound. This work helps to understand the influence of ultrasound in the QDs synthesis process and open up a new guidance for the preparation of high-quality QDs via interfacial reaction.

CRediT authorship contribution statement

Zongbo Zhang: Conceptualization, Data curation, Writing – original draft, Writing – review & editing. **Changbin Xu:** Data curation, Formal analysis, Visualization, Writing – original draft. **Shiliang Song:** . **Yan Ding:** . **Nan Meng:** . **Xuesheng Liu:** . **Yuan Zhang:** . **Liang Gong:** . **Wenting Wu:** .

Declaration of Competing Interest

The authors declare that they have no known competing financial interests or personal relationships that could have appeared to influence the work reported in this paper.

Appendix A. Supplementary data

Supplementary data to this article can be found online at https://doi.org/10.1016/j.ultsonch.2023.106411.

References

[1] S. Qu, Q. Jia, Z. Li, Z. Wang, L. Shang, Chiral NIR-II fluorescent Ag_2S quantum dots with stereospecific biological interactions and tumor accumulation behaviors, Sci. Bull. 67 (2022) 1274–1283.
[2] J.J. Ma, M.X. Yu, Z. Zhang, W.G. Cai, Z.L. Zhang, H.L. Zhu, Q.Y. Cheng, Z.Q. Tian, D.W. Pang, Gd-DTPA-coupled Ag_2Se quantum dots for dual-modality magnetic resonance imaging and fluorescence imaging in the second near-infrared window, Nanoscale 10 (2018) 10699–10704.
[3] C. Ding, Y. Huang, Z. Shen, X. Chen, Synthesis and Bioapplications of Ag_2S Quantum Dots with Near-Infrared Fluorescence, Adv. Mater. 33 (2021) 2007768.
[4] H.Y. Yang, Y.W. Zhao, Z.Y. Zhang, H.M. Xiong, S.N. Yu, One-pot synthesis of water-dispersible Ag_2S quantum dots with bright fluorescent emission in the second near-infrared window, Nanotechnology 24 (2013) 55706.
[5] S. Tsuboi, T. Jin, Fluorescent, Recombinant-Protein-Conjugated, Near-Infrared-Emitting Quantum Dots for in Vitro and in Vivo Dual-Color Molecular Imaging, Chembiochem 20 (2018) 568–575.
[6] Y. Du, B. Xu, T. Fu, M. Cai, F. Li, Y. Zhang, Q. Wang, Near-Infrared Photoluminescent Ag_2S Quantum Dots from a Single Source Precursor, J. Am. Chem. Soc. 132 (2010) 1470–1471.
[7] M. Gao, H. Zhao, Z. Wang, Y. Zhao, X. Zou, L. Sun, Controllable preparation of Ag_2S quantum dots with size-dependent fluorescence and cancer photothermal therapy, Adv. Powder Technol. 32 (2021) 1972–1982.
[8] Z. Deng, M. Jiang, Y. Li, H. Liu, S. Zeng, J. Hao, Endogenous H_2S-Triggered In Situ Synthesis of NIR-II-Emitting Nanoprobe for In Vivo Intelligently Lighting Up Colorectal Cancer, iScience, 17(2019) 217-224.
[9] Y. Shu, J. Yan, Q. Lu, Z. Ji, D. Jin, Q. Xu, X. Hu, Pb ions enhanced fluorescence of Ag_2S QDs with tunable emission in the NIR-II window: Facile one pot synthesis and their application in NIR-II fluorescent bio-sensing, Sens. Actuators B Chem. 307 (2020), 127593.
[10] H. He, Y. Lin, Z. Tian, D. Zhu, Z. Zhang, D. Pang, Ultrasmall Pb:Ag_2S Quantum Dots with Uniform Particle Size and Bright Tunable Fluorescence in the NIR-II Window, Small 14 (2018) 1703296.
[11] Y. Wang, X. Yan, Fabrication of vascular endothelial growth factor antibody bioconjugated ultrasmall near-infrared fluorescent Ag_2S quantum dots for targeted cancer imaging in vivo, Chem. Commun. 49 (2013) 3324.

[12] F. Wu, Y. Zhou, J. Wang, Y. Zhuo, R. Yuan, Y. Chai, A novel electrochemiluminescence immunosensor based on Mn doped Ag_2S quantum dots probe for laminin detection, Sens. Actuators B Chem. 243 (2017) 1067–1074.
[13] M. Geravand, F. Jamali-Sheini, Synthesis and physical properties of un- and Zn-doped Ag_2S nanoparticles, Adv. Powder Technol. 30 (2019) 347–358.
[14] V. Hakke, S. Sonawane, S. Anandan, S. Sonawane, M. Ashokkumar, Process Intensification Approach Using Microreactors for Synthesizing Nanomaterials—A Critical Review, Nanomaterials-Basel 11 (2021) 98.
[15] B. Prakash, V. Katoch, A. Shah, M. Sharma, M.M. Devi, J.J. Panda, J. Sharma, A. K. Ganguli, Continuous flow reactor for the controlled synthesis and inline photocatalysis of antibacterial Ag_2S nanoparticles, Photochem. Photobiol. 96 (2020) 1273–1282.
[16] S. Xue, T. Zhang, X. Wang, Q. Zhang, S. Huang, L. Zhang, L. Zhang, W. Zhu, Y. Wang, M. Wu, Q. Zhao, P. Li, W. Wu, Cu, Zn Dopants Boost Electron Transfer of Carbon Dots for Antioxidation, Small 17 (2021) 2102178.
[17] Y. Shu, P. Jiang, D.W. Pang, Z.L. Zhang, Droplet-based microreactor for synthesis of water-soluble Ag_2S quantum dots, Nanotechnology 26 (2015), 275701.
[18] Y.M. Zeng, L.J. Pan, J. Wang, Y.L. Fan, Y. Shu, D.W. Pang, Z.L. Zhang, Interfacial Synthesis of Ag_2S/ZnS Core/Shell Quantum Dots in a Droplet Microreactor, ChemistrySelect 5 (2020) 5889–5894.
[19] Z. Wang, T. Kadohira, T. Tada, S. Watanabe, Nonequilibrium quantum transport properties of a silver atomic switch, Nano Lett. 7 (2007) 2688–2692.
[20] Z. Luo, H. Zhang, J. Huang, X. Zhong, One-step synthesis of water-soluble $AgInS_2$ and ZnS-$AgInS_2$ composite nanocrystals and their photocatalytic activities, J. Colloid Interf. Sci. 377 (2012) 27–33.
[21] X. Zhong, Y. Feng, Y. Zhang, Facile and Reproducible Synthesis of Red-Emitting CdSe Nanocrystals in Amine with Long-Term Fixation of Particle Size and Size Distribution, J. Phys. Chem. C 111 (2007) 526–531.
[22] F. Heydaripour, M. Molaei, M. Karimipour, F. Dehghan, E. Mollahosseini, Conversion of the yellow to blue emission of CdSe quantum dots (QDs) via ZnSe shell growth, J. Mater. Sci. Mater. Electron. 30 (2019) 11378–11382.
[23] A.H. Gore, A.L. Prajapat, Biopolymer Nanocomposites for Sustainable UV Protective Packaging, Front. Mater. 9 (2022).
[24] L. Da Rosa, I. Aversa, E. Raphael, A. Polo, A. Duarte, M. Schiavon, L. Virtuoso, Improving Photoluminescence Quantum Yield of CdTe Quantum Dots Using a Binary Solvent (Water + Glycerin) in the One-Pot Approach Synthesis, J. Brazil. Chem. Soc. (2021).
[25] C.H. Chiang, T.Y. Li, H.S. Wu, K.Y. Li, C.F. Hsu, L.F. Tsai, P.K. Yang, Y.J. Lee, H. C. Lee, C.Y. Wang, M.L. Tsai, High-stability inorganic perovskite quantum dot-cellulose nanocrystal hybrid films, Nanotechnology 31 (2020), 324002.
[26] S. Yuan, Z. Wang, M. Zhuo, Q. Tian, Y. Jin, L. Liao, Self-Assembled High Quality CsPbBr 3 Quantum Dot Films toward Highly Efficient Light-Emitting Diodes, ACS Nano 12 (2018) 9541–9548.
[27] L. Chen, D. Chen, Y. Jiang, J. Zhang, J. Yu, C.C. DuFort, S.R. Hingorani, X. Zhang, C. Wu, D.T. Chiu, A BODIPY-Based Donor/Donor-Acceptor System: Towards Highly Efficient Long-Wavelength-Excitable Near-IR Polymer Dots with Narrow and Strong Absorption Features, Angew. Chem. Int. Ed. 58 (2019) 7008–7012.
[28] Q. Wu, M. Zhou, J. Shi, Q. Li, M. Yang, Z. Zhang, Synthesis of water-soluble Ag_2S quantum dots with fluorescence in the second near-infrared window for turn-on detection of Zn (II) and Cd (II), Anal. Chem. 89 (2017) 6616–6623.
[29] P. Jiang, C. Zhu, Z. Zhang, Z. Tian, D. Pang, Water-soluble Ag2S quantum dots for near-infrared fluorescence imaging in vivo, Biomaterials 33 (2012) 5130–5135.
[30] Y. Zhang, Y. Liu, C. Li, X. Chen, Q. Wang, Controlled Synthesis of Ag_2S Quantum Dots and Experimental Determination of the Exciton Bohr Radius, J. Phys. Chem. C 118 (2014) 4918–4923.
[31] X. Jiang, B.Q. Li, X. Qu, H. Yang, H. Liu, Thermal sensing with CdTe/CdS/ZnS quantum dots in human umbilical vein endothelial cells, J. Mater. Chem. B 5 (2017) 8983–8990.
[32] S. Zhao, C. Yao, Q. Zhang, G. Chen, Q. Yuan, Acoustic cavitation and ultrasound-assisted nitration process in ultrasonic microreactors: The effects of channel dimension, solvent properties and temperature, Chem. Eng. J. 374 (2019) 68–78.
[33] S. Zhao, Z. Dong, C. Yao, Z. Wen, G. Chen, Q. Yuan, Liquid-liquid two-phase flow in ultrasonic microreactors: Cavitation, emulsification, and mass transfer enhancement, AICHE J. 64 (2018) 1412–1423.
[34] T. Leong, M. Ashokkumar, S. Kentish, The growth of bubbles in an acoustic field by rectified diffusion, Springer (2016) 69–98.
[35] W. Lauterborn, T. Kurz, Physics of bubble oscillations, Rep. Prog Phys. 73 (2010), 106501.
[36] C. Zhang, X. Guo, L. Royon, P. Brunet, Acoustic Streaming Generated by Sharp Edges: The Coupled Influences of Liquid Viscosity and Acoustic Frequency, Micromachines-Basel 11 (2020) 607.
[37] Z. Zhang, K. Wang, C. Xu, Y. Zhang, W. Wu, C. Lu, W. Liu, Y. Rao, C. Jiang, C. Xu, S. Song, Ultrasound enhancing the mass transfer of droplet microreactor for the synthesis of AgInS2 nanocrystals, Chem. Eng. J. 435 (2022), 134948.
[38] M. Rahimi, O. Jafari, A. Mohammdifar, Intensification of liquid-liquid mass transfer in micromixer assisted by ultrasound irradiation and Fe_3O_4 nanoparticles, Chem. Eng. Process. 111 (2017) 79–88.
[39] X. Wang, Y. Wang, F. Li, L. Li, X. Ge, S. Zhang, T. Qiu, Scale-up of microreactor: Effects of hydrodynamic diameter on liquid–liquid flow and mass transfer, Chem. Eng. Sci. 226 (2020), 115838.